4

Modelling of Chemical Alteration of Cement Materials in Radioactive Waste Repository Environment

Daisuke Sugiyama
Nuclear Technology Research Laboratory,
Central Research Institute of Electric Power Industry
Japan

1. Introduction

Cement is a potential waste packaging, backfilling and constructing material for the disposal of radioactive waste. The physical properties of cement materials such as low permeability and low diffusivity in their matrices reduce the migration of radionuclides from a cementitious repository. Also, under a high-pH condition provided by the leaching of the components of cement hydrates, the solubility is low and the sorption distribution ratio is high for many radionuclides, so that the release of radionuclides from radioactive waste is restricted. Therefore, cement materials are expected to enable both the physical and chemical containments of long-term radioactive waste in disposal systems (TRU Coordination Office, 2000).

Under geological conditions, cement materials alter due to various reactions such as dissolution into groundwater and secondary mineral formation caused by chemical components in groundwater. The containment properties of cement materials are affected by these reactions. Also, the leached high-pH solution with alkaline components from the cement materials affects the physical and chemical properties of bentonite and the surrounding rocks. Therefore, for the long-term safety assessment of radioactive waste disposal, it is necessary to develop a methodology to estimate the long-term evolution of the cementitious repository system. The chemistry of the CaO-SiO_2-H_2O (C-S-H) system is a key parameter since it is suggested to be responsible for the high-pH condition in cements and is important in discussing the high-pH chemical condition in the long-term assessment of a repository environment (Atkinson et al., 1985; Atkinson, 1985). The author therefore has been developing a series of predictive calculation models based on a discussion of the incongruent dissolution/precipitation of the C-S-H system (Sugiyama & Fujita, 2006; Sugiyama et al., 2007; Sugiyama, 2008).

In this study, the alteration of cement materials in an underground repository environment is discussed. Cement materials come in contact with groundwater and some secondary minerals are expected to precipitate in the repository environment. The precipitation of calcite and its effects on the alteration of cement materials should be key issues in assessing the long-term performance of cement materials. There have been some experimental studies

on these issues, in which the precipitation of calcite from calcium bicarbonate solution passing through cracks in concrete and the leaching behaviour of components from cementitious materials were observed (Harris et al., 1998; Glasser et al., 2001). It was observed that calcite is mostly precipitated on the surface of the cracks, filling the cracks, and it was suggested that the thin layers of low-porosity calcite produced act as a diffusion barrier limiting contact between the cement and the solution (Harris et al., 1998; Glasser et al., 2001). Brodersen (2003) simulated the obtained experimental results using the CRACK2 computation model. Also, Lagneau and van der Lee (2005) simulated the clogging effect due to the precipitation of secondary minerals using the HYTEC code and showed that the precipitation leads to a reduction in porosity, which reduces the diffusive migration rate of chemical species. Burnol et al. (2005) discussed the precipitation behaviour of some minerals at a concrete/clay interface using various reactive transport codes. Marty et al. (2009) investigated the modelling of concrete/clay interactions under a geological disposal condition and discussed an occlusion due to the secondary mineral precipitation including calcite. However, the incongruent dissolution of the calcium-silicate hydrate (C-S-H) phase, which is one of the principle components of cementitious materials, was not sufficiently discussed in the previous modelling studies. Brodersen (2003) disregarded the leaching of silicic acid, and in the other studies, only three C-S-H phases (C-S-H 1.8, C-S-H 1.1 and C-S-H 0.8 (Lagneau & van der Lee, 2005; Burnol et al., 2005), and C-S-H 1.6, C-S-H 1.2 and C-S-H 0.8 (Marty et al., 2009) were included discretely in their modelling.

In this study, a reactive transport computational code, in which a geochemical model including the thermodynamic incongruent dissolution model of C-S-H (Sugiyama & Fujita, 2006) is coupled with the advection-diffusion/dispersion equation including the evolution of the hydraulic properties of the solid cement matrix due to the leaching and precipitation of components, has been developed. A series of experiments on the alteration of hydrated ordinary portland cement (OPC) and low-heat portland cement containing 30 wt% fly ash (FAC) monoliths in deionised water and sodium bicarbonate ($NaHCO_3$) solution were carried out and the model was optimised on the basis of the observations. Using the developed code, some implications for the long-term performance assessment of radioactive waste disposal systems were discussed.

2. Development of calculation code CCT-P

2.1 Model description

A coupling transport and chemical equilibrium calculation code, coupled chemical equilibria-mass transport code for porous media (CCT-P), is developed to predict the alteration behaviour of cement materials. The calculations using CCT-P are performed with a two-step procedure involving a nonreactive transport step (using Eqs. (3)-(8)) followed by a chemical equilibrium calculation. All thermodynamic modelling calculations were carried out using the thermodynamic database HATCHES (Bond et al., 1997) Ver. NEA15.

The thermodynamic incongruent dissolution model of C-S-H, proposed by Sugiyama & Fujita (2006), is employed in the modelling approach. In this model, C-S-H is assumed to be a binary nonideal solid solution of $Ca(OH)_2$ and SiO_2, and the log K values of the model end members of the solid solution are given as functions of the Ca/Si ratio of C-S-H (Sugiyama & Fujita, 2006):

$$\log K_{\mathrm{s}} = \frac{1}{1+y}\cdot\log K_{\mathrm{s0}} - \frac{1}{1+y}\cdot\log\frac{1}{1+y} + \frac{y}{(1+y)^2}\cdot\left[A'_{\mathrm{s0}} + A'_{\mathrm{s1}}\left(\frac{1-y}{1+y}\right) + A'_{\mathrm{s2}}\left(\frac{1-y}{1+y}\right)^2\right], \quad (1)$$

$$\log K_{\mathrm{c}} = \frac{y}{1+y}\cdot\log K_{\mathrm{c0}} - \frac{y}{1+y}\cdot\log\frac{y}{1+y} + \frac{y}{(1+y)^2}\cdot\left[A'_{\mathrm{c0}} + A'_{\mathrm{c1}}\left(\frac{1-y}{1+y}\right) + A'_{\mathrm{c2}}\left(\frac{1-y}{1+y}\right)^2\right], \quad (2)$$

y = Ca/Si ratio in C-S-H, $\log K_{\mathrm{s0}} = -2.710$, $\log K_{\mathrm{c0}} = 22.81$ (Bond et al., 1997).

At Ca/Si ≤ 0.461, $\log K_{\mathrm{s}} = \log K_{\mathrm{s0}} - \log(1+y)$.

At $1.755 \leq$ Ca/Si, $\log K_{\mathrm{s}} = -7.853$, $\log K_{\mathrm{c}} = 22.81$.

The fitted empirical parameters (A_{ij}) are shown in Table 1. This model can predict the equilibria of the incongruent dissolution and precipitation with a continuous change in the Ca/Si ratio of the solid phase by a series of calculations, in which the quantities of the dissolved/precipitated end members are calculated stepwisely, so that the quantities and compositions of the solid and liquid phases and the conditional solubility constants used in the next step can be estimated (Sugiyama & Fujita, 2006). CCT-P contains the geochemical code PHREEQE (Parkhurst et al., 1980) to calculate the chemical equilibrium, and the C-S-H model is employed to calculate the incongruent dissolution and precipitation by iterative calculations, because the simplicity of its numerical description allows its inclusion in chemical equilibrium calculations based on the common approach of using the law of mass action (log K) in PHREEQE (Parkhurst et al., 1980).

Fig. 1 (a) shows a schematic representation of the transport model used in CCT-P. To calculate the mass transport in the porous media, a one-dimensional advection /dispersion/diffusion equation is employed in CCT-P:

$$\frac{\partial}{\partial x}\{D_e(x,t)\cdot\frac{\partial C(x,t)}{\partial x}\} - V_d\cdot\frac{\partial C(x,t)}{\partial x} = \frac{\partial\{\phi(x,t)\cdot R_d(x,t)\cdot C(x,t)\}}{\partial t} - S_{eq}(x,t)\,, \quad (3)$$

where
C: concentration of aqueous species,
t : time,
ϕ : porosity,
V_d : velocity of flow in matrix,
D_e : effective diffusion coefficient in matrix,
S_{eq} : source term given by chemical equilibrium calculation within matrix,
R_d : retardation factor ($R_d(t) = 1 + \rho\cdot K_d\cdot\left(\frac{1-\phi(t)}{\phi(t)}\right)$),
ρ : density,
K_d : distribution coefficient.

End member	SiO_2			$Ca(OH)_2$		
A_{ij}	A_{s0}	A_{s1}	A_{s2}	A_{c0}	A_{c1}	A_{c2}
Ca/Si ≤ 0.833	-18.623	57.754	-58.241	37.019	-36.724	164.17
Ca/Si > 0.833	-18.656	49.712	25.033	36.937	-7.8302	-50.792

Table 1. Fitted values of empirical parameters (Sugiyama & Fujita, 2006)

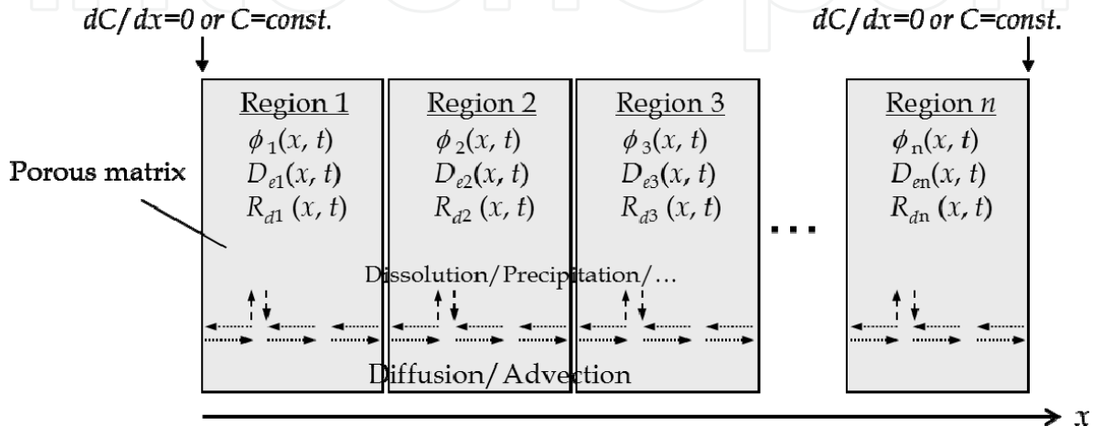

(a) Schematic representation of transport model

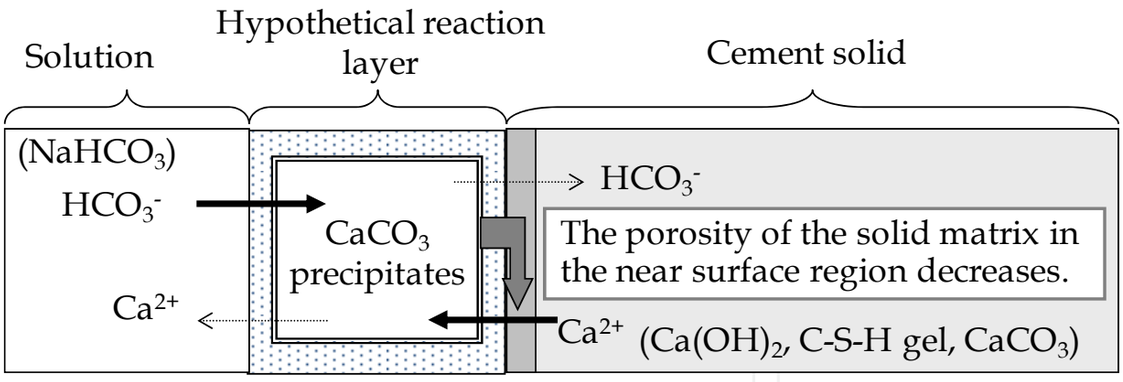

(b) Schematic representation of hypothetical reaction layer model

Fig. 1. Transport model in CCT-P

The evolution of the hydraulic properties of the solid cement matrix due to the leaching and precipitation of components is also considered in the calculation code. The component minerals in the solid are leached from its surface into the solution, and are precipitated on the surface and in the matrix of the solid. In this study, it is considered that the porosity of the solid matrix increases or decreases as the component minerals are dissolved and leached or precipitated, respectively. This is described by the following equations:

$$\phi(t) = 1 - (1 - \phi(0)) \cdot \frac{V_{solid}(t)}{V_{solid}(0)}, \tag{4}$$

$$V_{solid}(t) = \sum_{i:solid} CS_i(t) \cdot v_{mol_i} + V_{solid,static}, \tag{5}$$

where
V_{solid}: volume of solid phase,
CS: molarity of component mineral,
v_{mol}: molar volume of component mineral ($v_{mol\ Ca(OH)2}$ = 0.0331 dm^3 mol^{-1}, $v_{mol\ SiO2}$ = 0.0273 dm^3 mol^{-1}, $v_{mol\ CaCO3}$ = 0.0369 dm^3 mol^{-1}),
$V_{solid,static}$: volume of insoluble residual solid phase.

In CCT-P, the diffusion coefficient in the altered region of the solid matrix can be described as a function of porosity using formulas based on the study by Haga et al. (2005):

$$D(t) = D(0) \cdot \left(\frac{\phi(t)}{\phi(0)} \right)^n. \tag{6}$$

In this study, n = 2 (Haga et al., 2005) is assumed when calculating the evolution of the diffusion coefficient.

At the boundaries of the regions (Fig. 1 (a)), the advection/dispersion/diffusion equations (Eq. (3)) in adjacent regions are connected as follows:

$$J_{inner} = J_{outer} \tag{7}$$

where

J: flux of aqueous species,

$$J_{inner} = -D_e(x,t)_{inner} \cdot \left. \frac{\partial C(x,t)}{\partial x} \right|_{inner} + V_{d_{inner}} \cdot C(x,t)_{boundary},$$

$$J_{outer} = -D_e(x,t)_{outer} \cdot \left. \frac{\partial C(x,t)}{\partial x} \right|_{outer} + V_{d_{outer}} \cdot C(x,t)_{boundary}.$$

The subscripts *inner* and *outer* denote the values in the adjacent inner and outer cells, respectively.

In this study, the effects of the precipitation of calcite on the alteration of cement material are discussed. In the experiment, it was observed that calcite was mostly precipitated on the surface of the cement monolith, and the thin layers of low-porosity calcite produced acted as a diffusion barrier limiting contact between the solid cement and the solution (see subsection 4.1). Calcite precipitated in the pore solution of the cement solid matrix and also in the bulk solution near the interface between the cement solid and the solution. To describe this, a hypothetical reaction layer model is proposed and included in CCT-P, as shown in Fig. 1 (b). In this model, a less-soluble or insoluble secondary phase is formed in a

hypothetical reaction layer and precipitates in the vicinity of the surface of a solid phase. A hypothetical reaction layer is added between the solid and solution phases (outside of the solid phase interested), and calcium ions leached from the solid cement react with bicarbonate ions in the hypothetical reaction layer to form calcite. The formed calcite precipitates on the surface of the solid cement and the porosity of the solid matrix in the near-surface region decreases, then the precipitated layer of low-porosity restricts the diffusion mass transfer. This is described by the following equation:

$$-D_e(x,t)_{cement}\cdot\left.\frac{\partial C(x,t)}{\partial x}\right|_{cement}=\left(\frac{\phi(t)}{\phi(0)}\right)_{surface}\cdot\left\{-D_e(x,t)_{HRL}\cdot\left.\frac{\partial C(x,t)}{\partial x}\right|_{HRL}\right\}, \tag{8}$$

where the subscripts *cement*, *surface* and *HRL* denote the bulk cement region, the near-surface layer of the cement region in which the porosity decreases and the hypothetical reaction layer, respectively. $\phi(t)_{\text{surface}}$ is calculated using Eq. (4), assuming that all secondary precipitates formed in the HRL precipitate on the near-surface layer with a thickness of L_{shell} and contribute to adjust porosity. The thickness of the near-surface layer (L_{shell}) is provided as a parameter in CCT-P. Note that the code refers to $\phi(t)_{\text{surface}}$ only in calculations using Eq. (8) connecting regions at the boundary. The term $(\phi(t)/\phi(0))_{\text{surface}}$ is used to describe that contact between the solid cement and the solution is limited by the calcite precipitate, which acts as a barrier.

2.2 Numerical method

The one-dimensional advection/dispersion/diffusion equation (Eq. (3)) employed in CCT-P is numerically solved by an implicit finite-difference method. Eq. (3) can be described in the generic form

$$\frac{\partial C_i}{\partial t}=A\frac{\partial^2 C_i}{\partial x^2}-B\frac{\partial C_i}{\partial x}-CC\cdot C_i+D, \tag{9}$$

where

$$A=\frac{D_e(x,t)}{\phi(x,t)\cdot R_d(x,t)},$$

$$B=\frac{1}{\phi(x,t)\cdot R_d(x,t)}\left\{-\frac{\partial D_e(x,t)}{\partial x}+V_d\right\},$$

$$CC=\frac{1}{\phi(x,t)\cdot R_d(x,t)}\cdot\frac{\partial\{\phi(x,t)\cdot R_d(x,t)\}}{\partial t},$$

$$D=\frac{S_{eq}(x,t)}{\phi(x,t)\cdot R_d(x,t)}.$$

The finite-difference equation for Eq. (9) is given as

$$-a_j C_{j-1}^n+b_j C_j^n-c_j C_{j+1}^n=d_j, \tag{10}$$

$$d_j = a_j C_{j-1}^o + b_j^* C_j^o + c_j C_{j+1}^o + D_j \cdot (\Delta x_j + \Delta x_{j+1}) , \tag{11}$$

j = 2, . . . N-1. (N: total number of meshes)

a_j, b_j, c_j and b^*_j are given as

$$a_j = \frac{A_j}{\Delta x_j} - \frac{1}{2} B_j ,$$

$$b_j = A_j \cdot (\frac{1}{\Delta x_j} + \frac{1}{\Delta x_{j+1}}) + \frac{1}{2} CC_j \cdot (\Delta x_j + \Delta x_{j+1}) + \frac{1}{\Delta t} (\Delta x_j + \Delta x_{j+1}) ,$$

$$c_j = \frac{A_j}{\Delta x_{j+1}} - \frac{1}{2} B_j ,$$

$$b_j^* = -A_j \cdot (\frac{1}{\Delta x_j} + \frac{1}{\Delta x_{j+1}}) - \frac{1}{2} CC_j \cdot (\Delta x_j + \Delta x_{j+1}) + \frac{1}{\Delta t} (\Delta x_j + \Delta x_{j+1}) .$$

Spatial discretization is performed by centered-in-space differencing and temporal discretization is performed by Crank-Nicholson (centered-in-time) differencing. A, B, CC and D in Eq. (9) are also described as the differenced forms

$$A_j = \frac{D_{e\,j}}{\phi_j \cdot R_{d\,j}} ,$$

$$B_j = \frac{1}{\phi_j \cdot R_{d\,j}} \{ - \frac{D_{e\,j+1} - D_{e\,j}}{\Delta x_j} + V_d \} ,$$

$$CC_j = \frac{1}{\phi_j \cdot R_{d\,j}} \cdot \frac{\phi_j^n \cdot R_d{}_j^n - \phi_j^o \cdot R_d{}_j^o}{\Delta t} ,$$

$$D_j = \frac{S_{eq\,j}}{\phi_j \cdot R_{d\,j}} .$$

(The superscripts ‘n’ and ‘o’ denote the newest value and an old value obtained at t-Δt, respectively. Porosity, effective diffusion coefficient and retardation factor without superscript are the newest values.)

For the boundary condition, the finite-difference equations are given as follows.

Upper boundary (Dirichlet boundary condition)

$$b_1 C_1^n - c_1 C_2^n = d_1 , \tag{12}$$

$$d_1 = a_1 (C_b^n + C_b^o) + b_1^* C_1^o + c_1 C_2^o + D_1 \cdot (\Delta x_1 + \Delta x_2) . \tag{13}$$

Upper boundary (Flux boundary condition)

$$(b_1 - a_1 \frac{\frac{D_{e,i}}{\Delta x_1}}{v_{db} + \frac{D_{e,i}}{\Delta x_1}}) C_1^n - c_1 C_2^n = d_1 \,, \tag{14}$$

$$d_1 = a_1 \frac{J_b^n + J_b^o}{v_{db} + \frac{D_{e,i}}{\Delta x_1}} + \left[\frac{a_1 \frac{D_{e,i}}{\Delta x_1}}{v_{db} + \frac{D_{e,i}}{\Delta x_1}} + b_1^* \right] C_1^o + a_1 C_2^o + D_1 \cdot (\Delta x_1 + \Delta x_2) \,. \tag{15}$$

Lower boundary (Dirichlet boundary condition)

$$-a_{N-1} C_{N-2}^n + b_{N-1} C_{N-1}^n = d_{N-1} \,, \tag{16}$$

$$d_{N-1} = c_{N-1}(C_b^n + C_b^o) + a_{N-1} C_{N-2}^n + b_{N-1}^* C_{N-1}^o + D_{N-1} \cdot (\Delta x_{N-1} + \Delta x_N) \,. \tag{17}$$

Lower boundary (Neumann boundary condition)

$$-a_{N-1} C_{N-2}^n + (b_{N-1} - c_{N-1}) C_{N-1}^n = d_{N-1} \,, \tag{18}$$

$$d_{N-1} = a_{N-1} C_{N-2}^o + (b_{N-1}^* + c_{N-1}) C_{N-1}^o + D_{N-1} \cdot (\Delta x_{N-1} + \Delta x_N) \,. \tag{19}$$

At the boundaries of the regions, the advection/dispersion/diffusion equations in adjacent regions are connected using the following finite-diffusion equation:

$$\begin{aligned} &-\frac{D_{e,j-1}}{\Delta x_{j-1}} C_{j-1}^n + (\frac{D_{e,j-1}}{\Delta x_j} + \frac{D_{e,j}}{\Delta x_{j+1}} - v_{dj,inner} + v_{dj,outer}) C_j^n - \frac{D_{e,j}}{\Delta x_{j+1}} C_{j+1}^n \\ &= \frac{D_{e,j-1}}{\Delta x_j} C_{j-1}^o - (\frac{D_{e,j-1}}{\Delta x_j} + \frac{D_{e,j}}{\Delta x_{j+1}} - v_{dj,inner} + v_{dj,outer}) C_j^o - \frac{D_{e,j}}{\Delta x_{j+1}} C_{j+1}^o \,. \end{aligned} \tag{20}$$

In CCT-P, these equations are solved by the backward substitution method.

3. Experimental

3.1 Materials

A series of experiments on the alteration of hydrated cement monoliths in deionised water and sodium bicarbonate solution were carried out in this study. Solid monolith samples of ordinary portland cement (OPC) and low-heat portland cement containing 30 wt% fly ash (FAC) were prepared for use in a so-called tank leaching experiment.

The chemical compositions of OPC and FAC used in this study are shown in Table 2. The cement was hydrated at a water/cement clinker mixing ratio of 0.35. The hydrated materials were then cured in water at 50 °C to enhance hydration (Taylor, 1997) and reduce the effects of unhydrated phases for 91 days.

The hydrated solid samples were analysed by X-ray diffraction (XRD). The results are shown in Table 3, and the predominant phases were portlandite, C-S-H gel and ettringite for all solid

cement hydrate samples. In FAC hydrate, XRD identified katoite ($Ca_3Al_2(SiO_4)(OH)_8$) as a minor mineral and quartz (SiO_2) as an unhydrated phase. The amount of $Ca(OH)_2$ in the hydrated solid samples was quantified by DTA and is shown in Table 3. The porosity of the solid matrix of cement samples and the pore size distribution were measured by mercury intrusion porosimetry, and these data are shown in Table 3 and Fig. 2.

3.2 Tank leaching experiment

Hardened OPC and FAC after curing were cut into 20 × 20 × 10 mm blocks using a diamond cutter. The cement monolith samples were set in the acrylic cells shown in Fig. 3 with a circular window of 12 mm diameter and placed in contact with the solution. The exposure of only one of the faces of each monolith to the aqueous solution in the alteration (leaching/precipitation) experiments simplifies the subsequent analysis of the distribution of components in the cement monolith. Each cell containing a cement monolith was placed in a vessel to which 80 cm^3 of deionised water or $NaHCO_3$ solution at room temperature was added. The initial concentrations of $NaHCO_3$ were 6×10^{-5}, 1×10^{-4}, 6×10^{-4}, 1×10^{-3}, and 6×10^{-3} mol dm^{-3}. The solution and solid samples were separated and the monolith samples were again placed in contact with fresh deionised water or $NaHCO_3$ solution after 1 week and then every 4-5 weeks. All experiments were prepared in nitrogen-filled glovebox in triplicates.

The concentrations of calcium and silica in each separated solution were measured by inductively coupled plasma atomic emission spectroscopy (ICP-AES) after passing it through a 0.45 μm membrane filter. Each filtered solution was acidified and diluted with known volumes of nitric acid (HNO_3) solution and distilled water before ICP-AES analysis to ensure that the concentrations of the target and matrix elements were appropriate for the analysis. The carbonate ion concentration in the solution was measured by ion chromatography. The surface of the monolith sample after 76 weeks was observed by scanning electron microscopy (SEM) and the cross section of the solid was analysed by energy-dispersive X-ray analysis (EDX analysis) to observe the distribution of components in a cement matrix.

Oxide composition / wt%	SiO_2	Al_2O_3	Fe_2O_3	CaO	MgO	SO_3	Na_2O	K_2O
OPC	21.4	5.4	2.7	64.8	1.5	2.1	0.3	0.5
FAC	32.9	9.5	3.8	46.9	1.2	1.9	0.8	0.6

Table 2. Oxide composition of cement clinker used in experiment

Sample	Minerals (Identified by XRD)	$Ca(OH)_2$ / wt% (Measured by DTA)	Porosity / % (Measured by mercury intrusion porosimetry)
OPC	$Ca(OH)_2$, C-S-H gel, Ettringite	17.4	12.0
FAC	$Ca(OH)_2$, C-S-H gel, Ettringite, Quarts, Katoite	4.0	28.9

Table 3. Analytical results of XRD, DTA and mercury intrusion porosimetry of hydrated cement sample

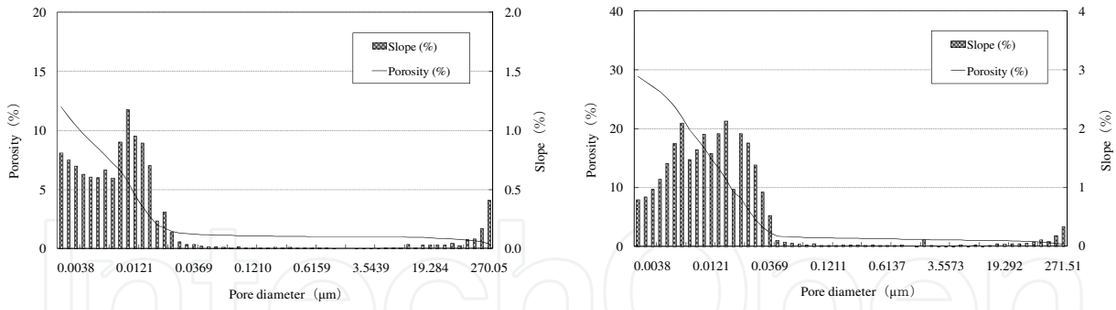

(a) OPC (b) FAC

Fig. 2. Pore size distributions of cement monolith samples

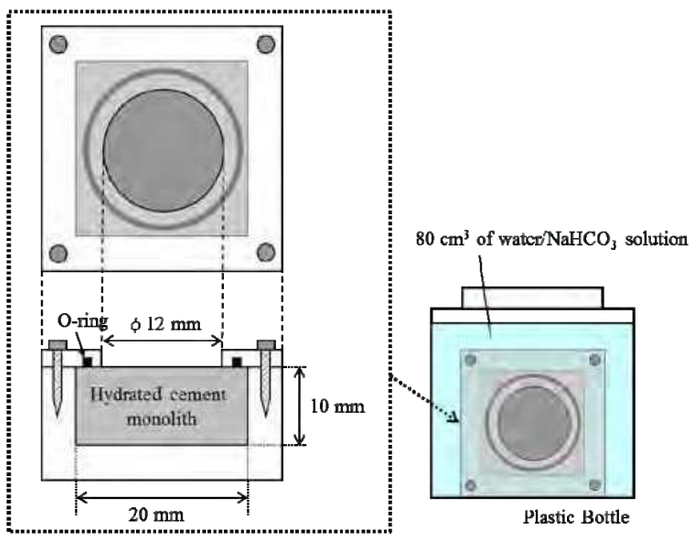

Fig. 3. Experimental cell for cement alteration experiment

4. Results

4.1 Cement monolith alteration experiments

The amount of calcium leached from the OPC monolith sample was calculated using the measured aqueous composition and is shown in Fig. 4 (a) as a function of time. In deionised water, calcium was leached from the surface of the OPC solid monolith and the leaching rate decreased slightly with time. This result suggests that in the early stage of alteration, the dissolution equilibrium of portlandite ($Ca(OH)_2$) dominated the leaching of calcium, and in the late stage, the incongruent dissolution of C-S-H gel in the altered surface region dominated the calcium leaching. In sodium bicarbonate solution at a $NaHCO_3$ concentration higher than 6×10^{-4} mol dm^{-3}, a reduction in the rate of calcium leaching was observed. As the concentration of $NaHCO_3$ increased, the rate of calcium leaching decreased and was restricted significantly in the later stage of the experiment. The leaching of calcium was always inhibited at the $NaHCO_3$ concentration of 6×10^{-3} mol dm^{-3} during the experiment.

In the FAC experiments shown in Fig. 4 (b), the trend of calcium leaching was observed to be similar to that in OPC experiments; however, the rate of calcium leaching was lower in the cases of FAC than in the cases of OPC. FAC inhibited the leaching of calcium in 6×10^{-4} mol dm^{-3} $NaHCO_3$ solution earlier than OPC. The leaching of calcium was inhibited from the early stage of the experiment at the $NaHCO_3$ concentration of $> 1 \times 10^{-3}$ mol dm^{-3}.

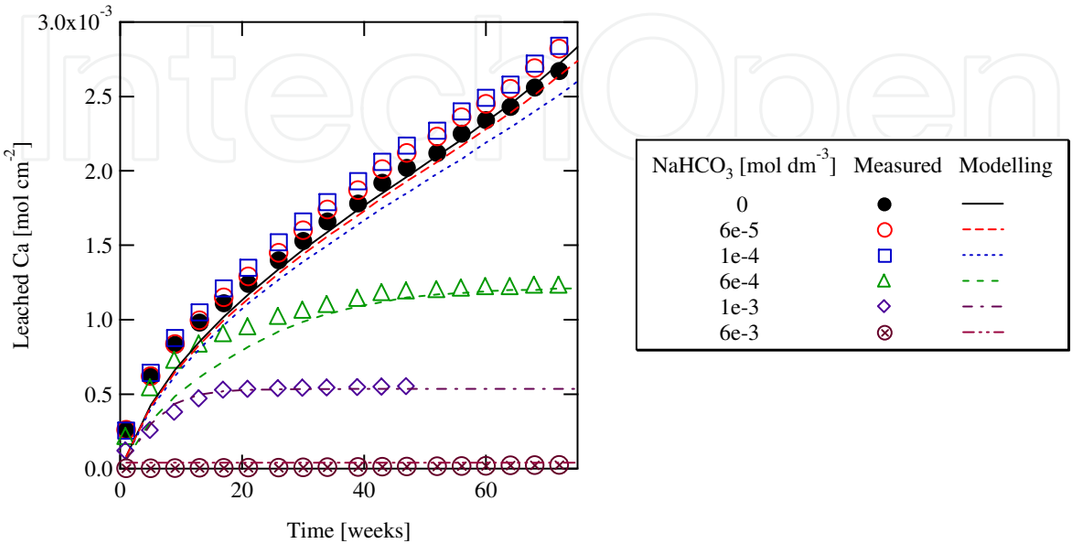

(a) OPC

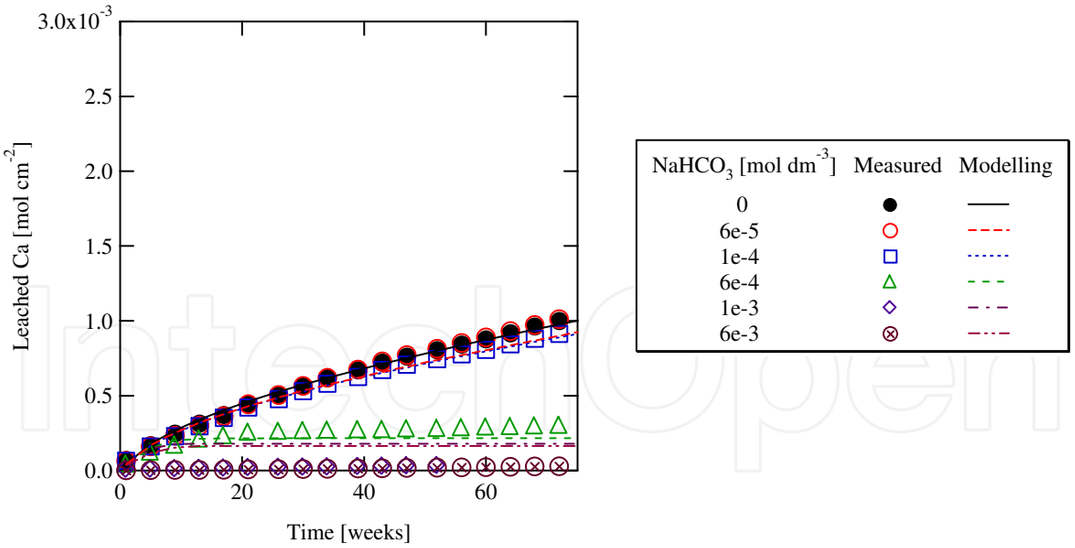

(b) FAC

Fig. 4. Measured and calculated amounts of calcium leached from cement monolith

For all the cases of alteration in $NaHCO_3$ solution, a secondary crystalline precipitate was formed on the surface of the solids, as shown in Fig. 5. The precipitate was identified as calcite by XRD analysis. A denser calcite layer was formed at higher $NaHCO_3$ concentrations of 1×10^{-3} and 6×10^{-3} mol dm^{-3}.

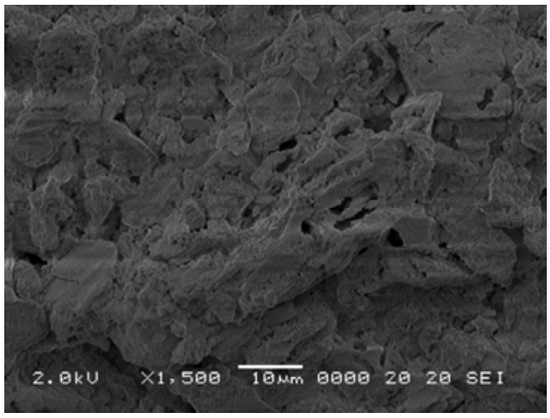

(a) OPC (in distilled water)

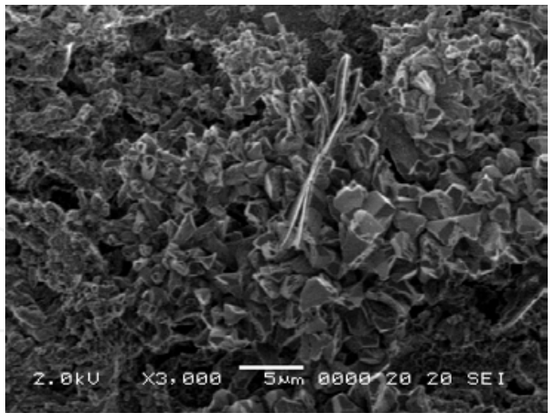

(b) OPC (in 1×10^{-4} mol dm^{-3} $NaHCO_3$)

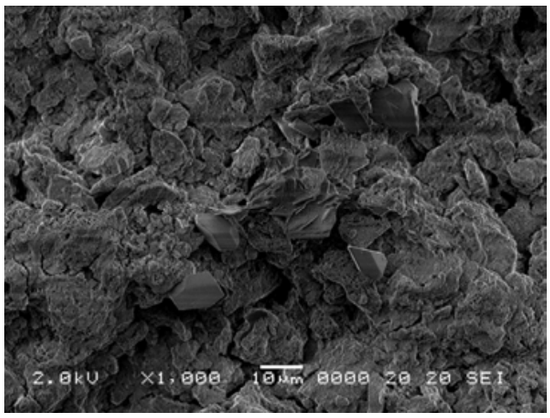

(c) OPC (in 6×10^{-4} mol dm^{-3} $NaHCO_3$)

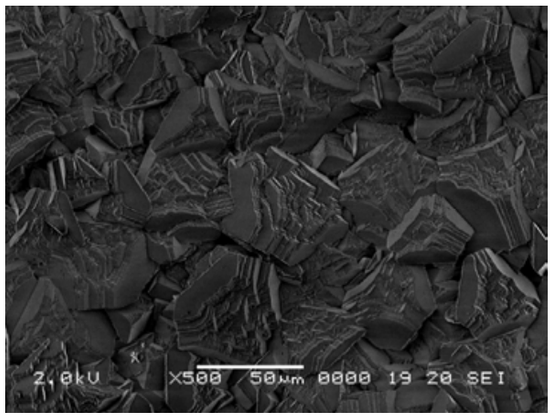

(d) OPC (in 6×10^{-4} mol dm^{-3} $NaHCO_3$) (Filmy layer of calcite precipitate)

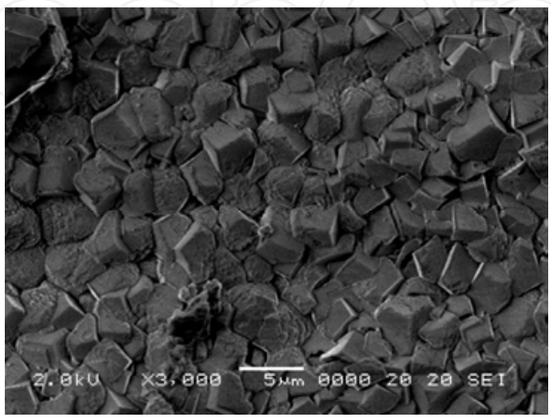

(e) OPC (in 6×10^{-3} mol dm^{-3} $NaHCO_3$)

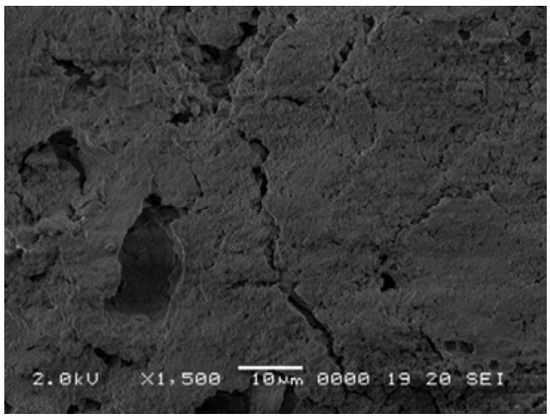

(f) FAC (in distilled water)

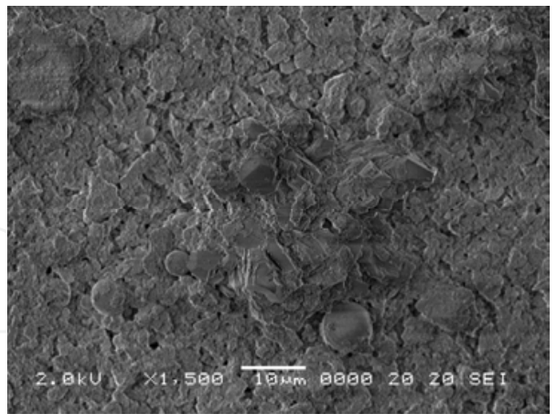

(g) FAC (in 1×10^{-4} mol dm^{-3} $NaHCO_3$)

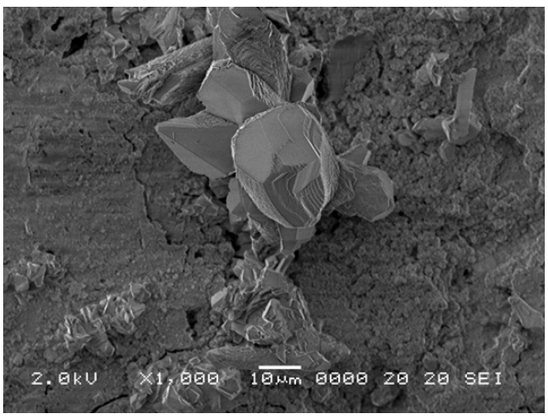

(h) FAC (in 6×10^{-4} mol dm^{-3} $NaHCO_3$)

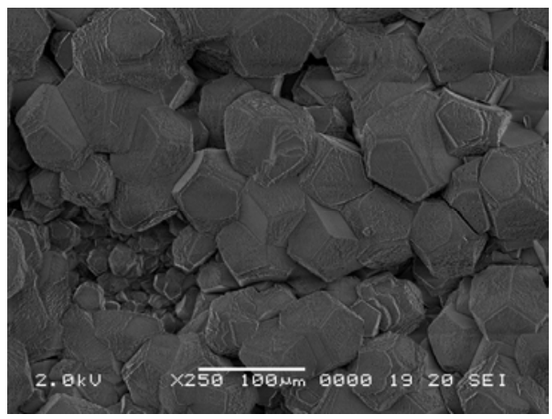

(i) FAC (in 6×10^{-4} mol dm^{-3} $NaHCO_3$)
(Filmy layer of calcite precipitate)

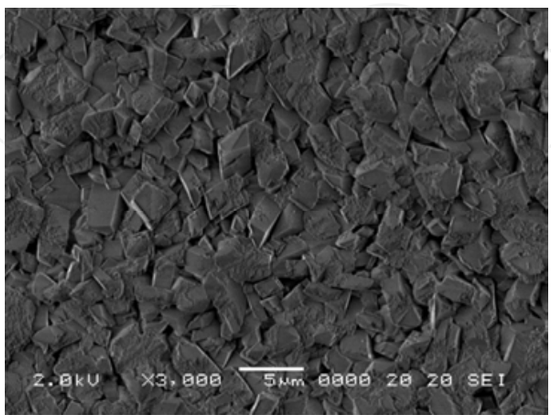

(j) FAC (in 6×10^{-3} mol dm^{-3} $NaHCO_3$)

Fig. 5. SEM observation on surface of cement monolith

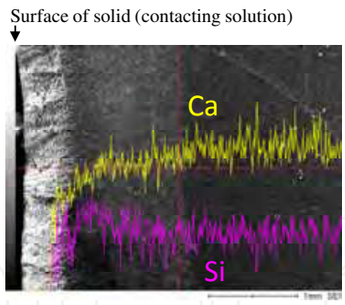

(a) OPC (in distilled water)

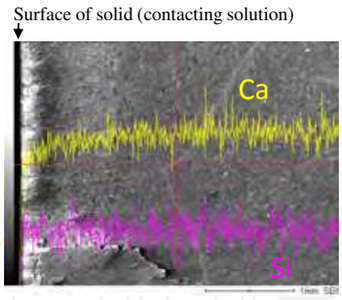

(b) OPC (in 6 × 10^{-4} mol dm^{-3} $NaHCO_3$)

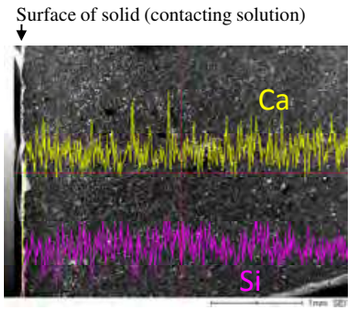

(c) OPC (in 6 × 10^{-3} mol dm^{-3} $NaHCO_3$)

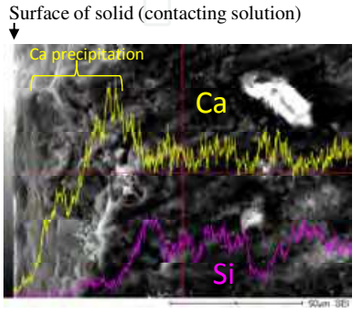

(d) OPC (in 6 × 10^{-3} mol dm^{-3} $NaHCO_3$) (Surface region)

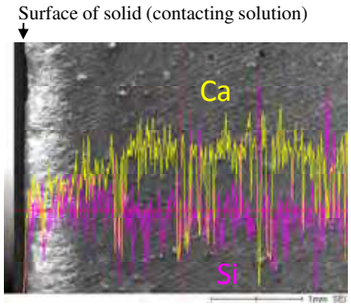

(e) FAC (in distilled water)

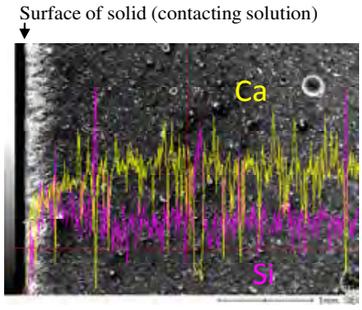

(f) FAC (in 6 × 10^{-4} mol dm^{-3} $NaHCO_3$)

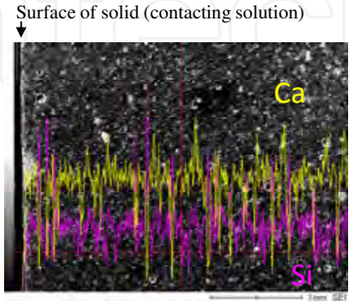

(g) FAC (in 6 × 10^{-3} mol dm^{-3} $NaHCO_3$)

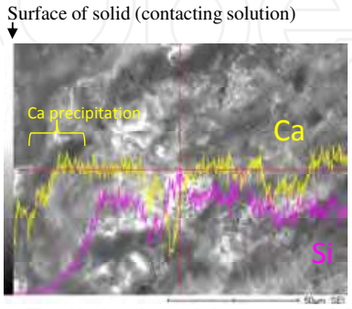

(h) FAC (in 6 × 10^{-3} mol dm^{-3} $NaHCO_3$) (Surface region)

Fig. 6. Calcium concentration profiles at cross section of altered cement sample after 76 weeks obtained by EDX analysis

The calcium concentration at the cross section of the divided altered solid samples analysed by EDX analysis is shown in Fig. 6. In deionised water, calcium was leached from the surface and the Ca/Si ratio of the solid decreased in the surface region up to a depth of around 2 mm. In sodium bicarbonate solution at a higher $NaHCO_3$ concentration of 6×10^{-4} mol dm^{-3}, the region with decreasing Ca/Si ratio of the solid was small up to a depth of around 1.0 mm. In contrast, it was observed that a small amount of calcium leached in 6×10^{-3} mol dm^{-3} sodium bicarbonate solutions. In 6×10^{-3} mol dm^{-3} $NaHCO_3$ solutions, a layer of accumulated calcium was formed at the vicinity of the surface of the solid, as shown in Figs. 6 (d) and (h). It is suggested that calcite precipitated on the surface of the monoliths in sodium bicarbonate solution and the secondary calcite precipitation concentrated in the near-surface layer. Thus, the secondary calcite precipitation restricted the leaching of calcium from the solid by limiting the contact between the solid cement and the solution.

The amount of calcite precipitated on the cement monolith sample was calculated using the measured carbonate ion concentration in the separated solution and is shown in Fig. 7 as a function of time. In $< 6 \times 10^{-4}$ mol dm^{-3} $NaHCO_3$ solutions, more calcite precipitated at higher $NaHCO_3$ concentrations. In the cases where a restriction of calcium leaching in $> 6 \times 10^{-4}$ mol dm^{-3} $NaHCO_3$ solutions was observed, the calcite precipitation rate decreased.

4.2 Modelling calculation of cement alteration experiment

The cement alteration experiments were simulated using the developed model and the CCT-P calculation code. First, the mineral compositions of the hydrated cements were derived by an approach based on that described by Glasser et al. (1987) with some modifications. Glasser et al. calculated the equilibrium phase distribution by considering the phases of $Ca(OH)_2$, C-S-H, hydrotalcite and monosulphate (Glasser et al., 1987). The hydrated OPC and FAC in the experiments were dominantly composed of portlandite, C-S-H gel, ettringite and a small amount of other minerals, and the amount of portlandite was measured by DTA. Thus, in this study, the mineral compositions of the hydrated OPC and FAC were calculated by the following approach.

For OPC:

Step 1. The mineral assembly in the hydrated OPC was described with portlandite ($Ca(OH)_2$), C-S-H, ettringite, brucite ($Mg(OH)_2$), NaOH and KOH. Na_2O, K_2O and MgO were assumed to be completely hydrated to NaOH, KOH and brucite, respectively.

Step 2. The amount of portlandite was estimated by DTA of the hydrated OPC sample used in the experiment in this study.

Step 3. SiO_2 was assumed to be taken up by the C-S-H gel with Ca/Si = 1.755 (Sugiyama & Fujita, 2006), and C-S-H was described using the model proposed by Sugiyama and Fujita (2006).

Step 4. The remaining CaO was assumed to be taken up by ettringite. The remaining Al_2O_3 was assumed to be amorphous alumina gel or taken up by some phases (e.g., C-A-S-H gel), although no excess Al was included in the following modelling calculations.

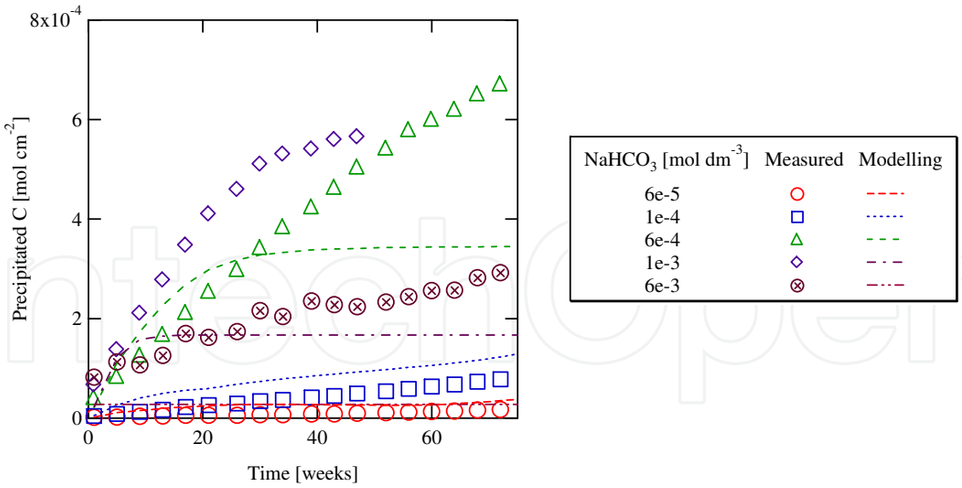

(a) OPC

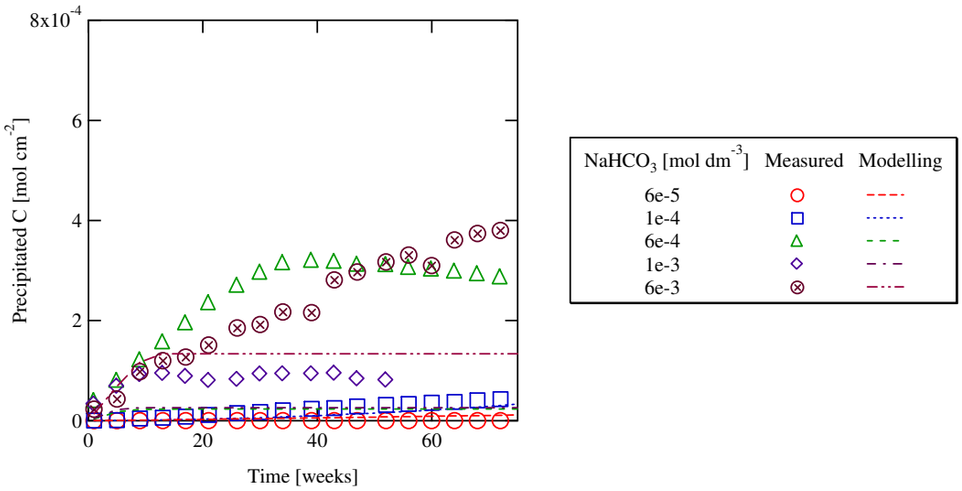

(b) FAC

Fig. 7. Measured and calculated amounts of calcite precipitated on cement monolith

For FAC:

Step 1. The mineral assembly in the hydrated FAC was described with portlandite ($Ca(OH)_2$), C-S-H, ettringite, brucite, katoite, NaOH, KOH and quartz. Na_2O, K_2O and MgO were assumed to be completely hydrated to NaOH, KOH and brucite, respectively.

Step 2. SO_3 was assumed to be taken up by ettringite. The remaining Al_2O_3 was assumed to be taken up by katoite.

Step 3. The remaining CaO was assumed to be taken up by portlandite and C-S-H gel with Ca/Si = 1.755 (Sugiyama & Fujita, 2006). The amount of portlandite was estimated by DTA of the hydrated FAC sample used in the experiment in this study.

Step 4. SiO_2 was assumed to be taken up by the C-S-H gel with Ca/Si = 1.755 (Sugiyama & Fujita, 2006).

Step 5. The remaining SiO_2 was assumed to be quartz, which is an unhydrated component in fly ash.

The mineral compositions of the OPC and FAC hydrates calculated by the method above are shown in Table 4. Then, the cement hydrates are simply described as the assembly of $Ca(OH)_2$ and C-S-H gel in this modelling study to reduce the load of calculation.

The calculation system was defined using the parameters in Table 5 and the model in Fig. 8. A constant boundary condition was imposed at the surface of the solid, which described the experimental condition of the replacement of the solution, and at the other end, a closed boundary condition was prescribed. Diffusion transport was calculated and advection transport was not considered in this simulation. As described in subsection 2.1, the HRL was added at the boundary between the solid and the solution to simulate the calcite precipitation on the surface of the monolith in the model. The amount of calcium leached from the solid into the solution was calculated by integrating the flux of calcium at the surface of the solid ($x = 0$).

[mol kg^{-1}]

Cement	Quartz	Katoite	Brucite	Ettringite	$Ca(OH)_2$	C-S-H gel (Ca/Si = 1.755)	NaOH	KOH
OPC	-	-	0.28	0.29	2.35	2.76	0.07	0.08
FAC	1.65	0.72	0.25	0.07	0.54	2.27	0.21	0.10

Table 4. Calculated mineral compositions of cement hydrates

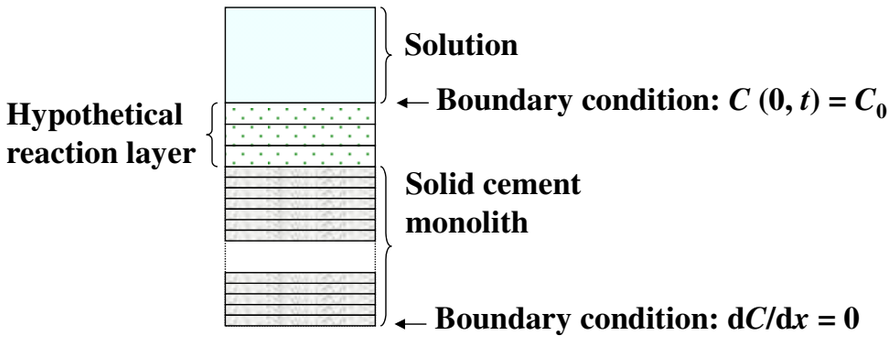

Fig. 8. Analysis model used for OPC alteration experiment

Cement		OPC	FAC
Hypothetical reaction layer (HRL)	Thickness of region [mm]	0.3	0.3
	Thickness of each grid layer [mm]	0.1	0.1
	Initial D_e [m^2 s^{-1}]	$8.0 \times 10^{-10*}$	$8.0 \times 10^{-10*}$
Cement hydrate solid	Thickness of region [mm]	10	10
	Thickness of each grid layer [mm]	0.267	0.200
	Initial D_e [m^2 s^{-1}]	$1.9 \times 10^{-11**}$	$7.4 \times 10^{-12**}$
	Initial porosity	0.120	0.289

* An infinite dilution diffusion coefficient for calcium was assumed in the calculation.
** The initial effective diffusion coefficient in the cement solid matrix was provided by fitting calculation using the leaching data of calcium from the cement monolith in distilled water.

Table 5. Calculation parameters used for modelling OPC alteration experiment

The spatial resolution and the initial effective diffusion coefficient were optimised by preliminary sensitivity calculations to reproduce the rate of calcium leaching in the experiments in distilled water. The fitted initial effective diffusion coefficients given in Table 5 are comparable with the values measured by Haga et al. (2005) and Yasuda et al. (2002). The time step size was given in consideration of a Neumann criterion (Marty et al., 2009; Sousa, 2003; Hindmarsh & Gresho, 1984):

$$\frac{2D_p \cdot \Delta t}{\Delta x^2} \leq 1, \tag{21}$$

where D_p (= D_e/ϕ) is the pore diffusion coefficient, and Δx and Δt refer to the mesh size in the solid region and the time step.

For modelling using the two-step procedure, it is suggested that the choice of the space discretization affects the calculation results (Marty et al., 2009). In this study, the sensitivity of calculation to the mesh size was analysed. The sensitivity calculation results are shown in Fig. 9. In the case of OPC (Fig. 9 (a)), coarser mesh sizes gave a lower rate of calcium leaching and finer mesh sizes degraded the stability of numerical solutions. The optimised mesh size in this case is 0.267 mm, which reproduced the measured result using a diffusion coefficient (1.9×10^{-11} m^2 s^{-1}) compatible with the experimentally determined value (Haga et al., 2005). In the case of FAC (Fig. 9 (b)), the calculation result was less sensitive to the space discretization, though a behaviour similar to that of OPC was observed.

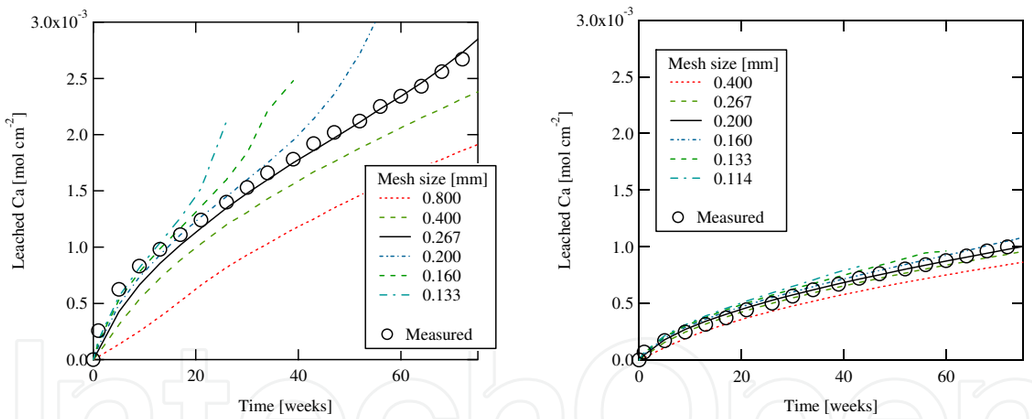

(a) OPC (b) FAC

Fig. 9. Sensitivity analysis of mesh size in solid region

The thickness of the HRL was optimised by sensitivity calculations given in Fig. 10. It is considered that a smaller HRL gives lesser disturbance to the calculation. The optimised HRL size was chosen to be 0.3 mm since too fine HRL could affect the stability of the numerical solution. It is noted that FAC calculation was insensitive to the HRL thickness (Fig. 10 (b)).

To model the alteration in the $NaHCO_3$ solutions, the thickness of the near-surface layer (L_{shell}) must be determined. Parametric analysis was carried in this study and is discussed in subsection 5.1. In this subsection, the best-fit results are described with the optimised L_{shell}

given in Table 6. As shown in Fig. 4, the modelling calculations quantitatively well predicted the experimental results for the leaching of calcium. Figure 7 shows that calcite precipitation was predicted fairly well at lower $NaHCO_3$ concentrations ($\leq 1 \times 10^{-4}$ mol dm^{-3}), though it was underestimated at higher $NaHCO_3$ concentrations. In the CCT-P calculation, the amount of precipitated calcite saturated after 10 ~ 20 weeks owing to clogging; however, in the experiments, calcite still precipitated even if the rate of precipitation decreased with time.

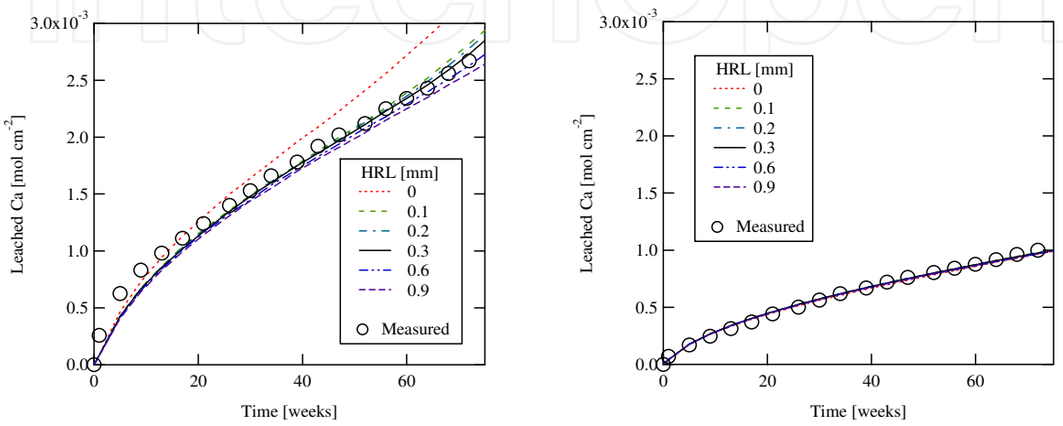

(a) OPC (b) FAC

Fig. 10. Sensitivity analysis of thickness of HRL

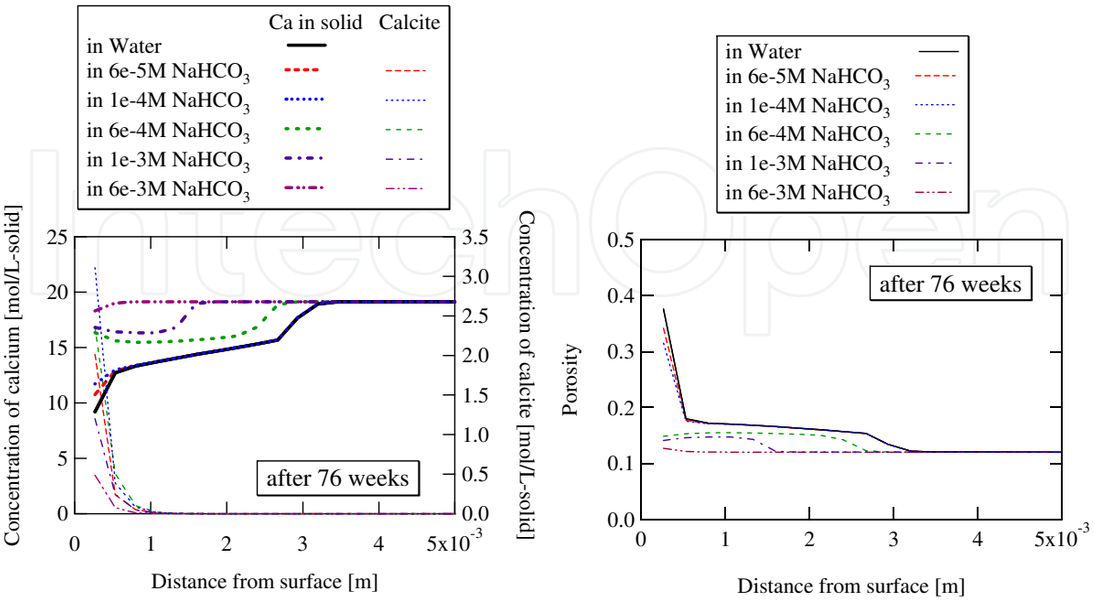

(a) OPC

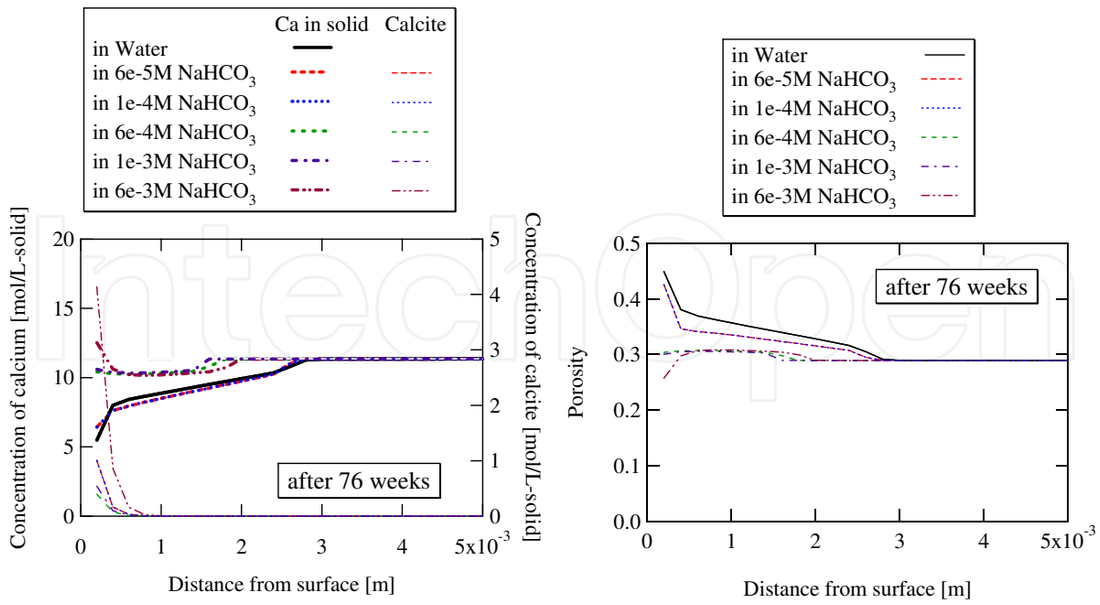

(b) FAC

Fig. 11. Results of calculation modelling alteration of cement monolith

The calculation also predicted qualitatively the calcium concentration in the solid matrix by comparing Fig. 11 with Fig. 6. The porosity in the altered region increased in distilled water, as shown in Fig. 11. The porosity decreased at the surface in $NaHCO_3$ solutions and little alteration in the porosity of the solid was predicted for 1×10^{-3} and 6×10^{-3} mol dm^{-3} $NaHCO_3$ solutions. In the case of FAC, a marked reduction in the porosity in the vicinity of the surface of the solid was predicted owing to calcite precipitation in the region.

5. Discussion

5.1 Mechanism of clogging

Figures 4 and 7 demonstrate that a higher $NaHCO_3$ concentration in a solution induces a larger reduction in the rate of calcium leaching from a cement hydrate monolith due to calcite precipitation. However, in some cases, more calcite did not always precipitate at higher $NaHCO_3$ concentrations; more calcite precipitated at the $NaHCO_3$ concentrations of 6×10^{-4} and 1×10^{-3} mol dm^{-3} than at the $NaHCO_3$ concentration of 6×10^{-3} mol dm^{-3} for OPC, as shown in Fig. 7 (a), and more calcite precipitated at the $NaHCO_3$ concentration of 6×10^{-4} mol dm^{-3} than at the $NaHCO_3$ concentrations of 1×10^{-3} and 6×10^{-3} mol dm^{-3} for FAC, as shown in Fig. 7 (b). These results also suggest that a denser calcite layer was formed at the higher $NaHCO_3$ concentrations and its effect of inhibiting the leaching of calcium was more notable owing to a stronger restriction on mass transport at the interface between the solid and the solution.

The behaviour above can be described using the thickness of the near-surface layer (L_{shell}) as a parameter. In the proposed model, all calcite formed in the solution (in the HRL) precipitates on the near-surface layer so that a denser calcite layer formed as calcite

concentrates in a thinner layer (smaller L_{shell}). Kurashige and Hironaga (2007) carried out a series of leaching experiments using OPC and low-heat portland cement in $NaHCO_3$ solution, and found that the secondary calcite precipitation layer grew thinner as the $NaHCO_3$ concentration increased. Based on their finding, it can be assumed that the thickness of the near-surface layer of calcite depends on the $NaHCO_3$ concentration in the solution. This assumption is discussed by the sensitivity analysis of L_{shell}, as shown in Fig. 12. Figure 12 demonstrates that a smaller L_{shell} gives a larger reduction in the rate of calcium leaching. Table 6 gives the best-fit values of the near-surface layer obtained by sensitivity analysis.

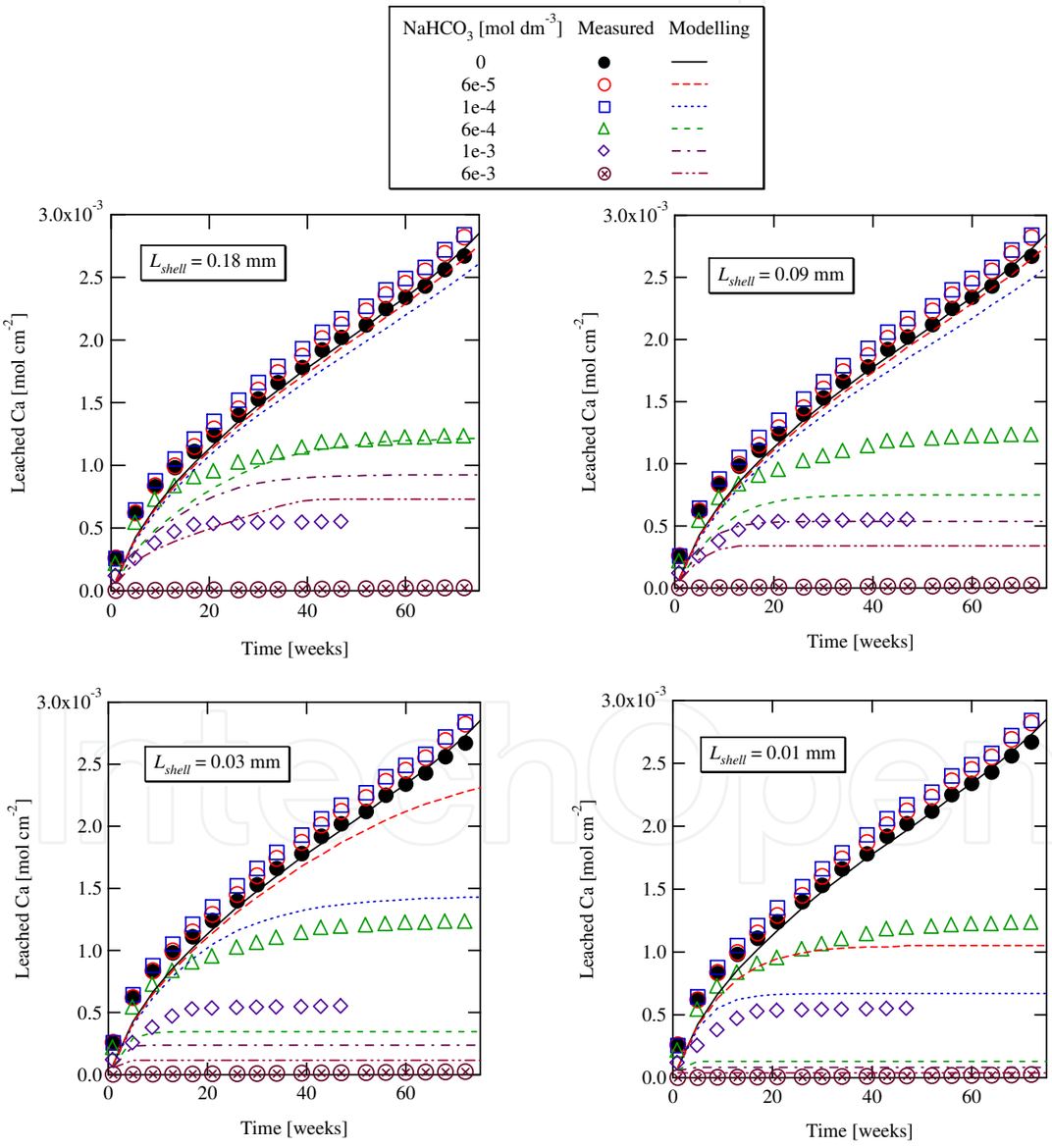

(a) OPC

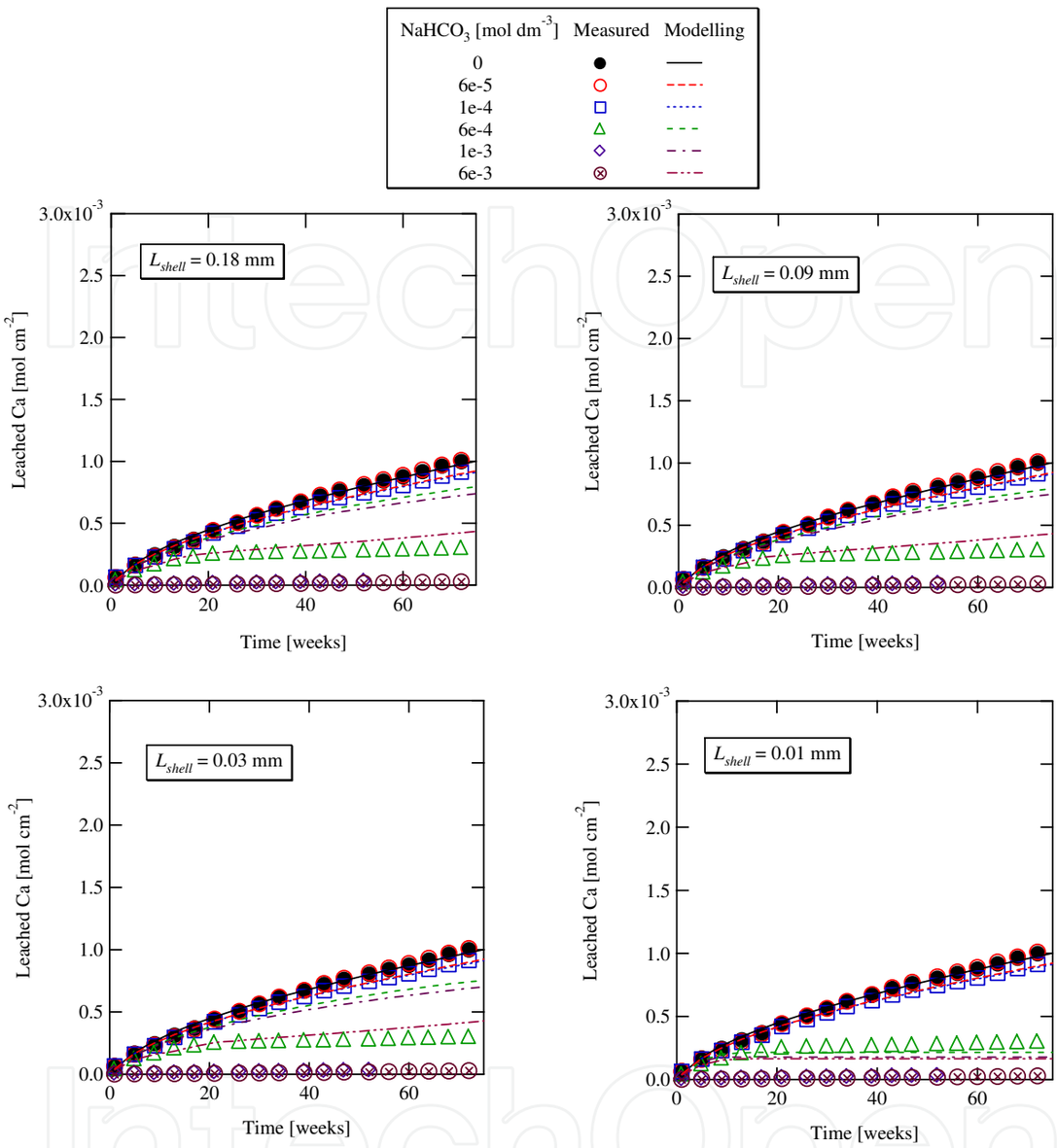

(b) FAC

Fig. 12. Results of sensitivity calculation of thickness of near-surface layer

In the case of FAC, the near-surface layer appears to be insensitive to $NaHCO_3$ concentration. It could be interpreted that the penetration of carbonate ions into the solid was restricted owing to the low diffusivity in the FAC matrix. It is noted that a lower diffusion coefficient was provided for FAC than for OPC even though the porosity of FAC (29%) was higher than that of OPC (12%). Similar observations were given by Sugiyama et al. (2008) and Chida and Sugiyama (2007, 2008): they observed that the effective diffusion coefficients of uranium (Sugiyama et al., 2008) , organic carbon (Chida and Sugiyama, 2008), caesium, strontium and iodine (Chida and Sugiyama, 2007) in the FAC matrix were more than an order of magnitude lower than those in the OPC matrix, though the porosity of FAC

was higher than that of OPC. The reason for the lower diffusion coefficients for FAC is still unclear, but it should be interpreted using the smaller pore size distribution in the FAC matrix (Chida and Sugiyama, 2007). Also, it could be suggested that the pore microstructure (tortuosity of the pore network) affected diffusivity (Promentilla, 2009). Further studies should be carried out to investigate the growth of the secondary precipitation layer to discuss the mechanism of clogging in more detail.

$NaHCO_3$ concentration [mol dm^{-3}]	L_{shell} for OPC [mm]	L_{shell} for FAC [mm]
6×10^{-5}	0.18	0.01
1×10^{-4}	0.18	0.01
6×10^{-4}	0.18	0.01
1×10^{-3}	0.09	0.01
6×10^{-3}	0.01	0.01

Table 6. Best-fit thickness of near-surface layer (L_{shell})

5.2 Extrapolation of modelling to assess long-term alteration of cementitious repository

It has been demonstrated that the proposed model in this study has the capability of describing the leaching of calcium with the incongruent dissolution of C-S-H and the effect of the precipitation of the secondary less soluble phase (calcite) on the alteration of cement materials. To extrapolate the modelling for the assessment of the long-term alteration of a cementitious repository in the underground repository environment, some issues should be discussed further to improve the reliability of the modelling calculation.

Temporal and spatial discretizations should be carefully optimised in the modelling. A finer mesh size could give a better, more accurate prediction as examined in subsection 4.2; however, the numerical calculation would be instable with a very fine (too small) mesh size, as shown in Fig. 9. It would be impractical to choose very fine spatial and temporal resolutions when considering the computing time for the simulation of the long-term (sometimes up to million years) alteration of an engineering-scale repository (more than tens of meters). A deliberate sensitivity analysis should be carried out to provide a credible assessment. Also, it is suggested that the choice of material could improve the quality of assessment since FAC was less sensitive to the temporal and spatial discretizations, and also the size of HRL according to the modelling results in this study. This could be interpreted on the basis of the low diffusivity in the FAC matrix.

Another important issue is the need to investigate the mechanism of clogging in more detail. In the underground environment, cementitious materials are placed in contact with groundwater through other engineering barrier materials or surrounding rocks. The rate of alteration could be moderated compared to the experiment in which the cement solid is placed in contact with the solution directly. Further experimentation is required on the alteration on the solid in an actual repository environment and enables us to establish optimised calculation conditions including spatial and temporal resolutions, the appropriate HRL, and the thickness of the near-surface layer (L_{shell}). In situ pilot experiments in the repository environment will be effective in tackling this issue.

6. Conclusions

A reactive transport computational code, in which a geochemical model including the thermodynamic incongruent dissolution model of C-S-H is coupled with the advection-diffusion/dispersion equation, was developed on the basis of a series of experiments on the alteration of hydrated cement monoliths in deionised water and in sodium bicarbonate solution. The code can describe the evolution of the hydraulic properties of the solid cement matrix due to the leaching and precipitation of components and the clogging effect by insoluble secondary phase precipitation that inhibits the alteration of cement materials.

The precipitation of secondary calcite on the surface of cement solid induces a reduction in the rate of components leaching. The clogging behaviour depends on the feature of the near-surface layer of precipitates, which is sensitive to the concentration of reactive ions in the solution and the mass transport property of the solid matrix. Further experimental studies are needed to analyse in detail the alteration at the interface between cementitious material and other barrier materials (e.g., bentonite and host rock) under actual underground repository conditions. FAC, in which a low diffusivity is given, is suggested to reduce the uncertainty in the long-term performance assessment.

7. References

Atkinson, A. (1985). *The Time Dependence of pH within a Repository for Radioactive Waste Disposal*, AERE R 11777, UKAEA, 1985.

Atkinson, A.; Goult, D.J. & Hearne, J.A. (1985). An Assessment of the Long-term Durability of Concrete in Radioactive Waste Repositories, *Scientific Basis for Nuclear Waste Management IX (Material Research Society Symposium Proceedings volume 50)*, pp. 239-246, Stockholm, Sweden, September 1985.

Bond, K.A.; Heath, T.G. & Tweed, C.J. (1997). *HATCHES: A Referenced Thermodynamic Database for Chemical Equilibrium Studies*, Nirex Report NSS/R379, 1997.

Brodersen, K. (2003). *CRACK2 – Modelling Calcium Carbonate Deposition from Bicarbonate Solution in Cracks in Concrete*, Risø-R-1143(EN), ISBN 87-550-2612-5, 2003.

Burnol, A.; Blanc, P.; Tournassat, C.; Lassin, A.; Xu, T. & Gaucher, E.C. (2005). Intercomparison of Reactive Transport Models Applied to Degradation of a Concrete/Clay Interface, *Migration '05*, Avignon, France, September 2005.

Chida, T. & Sugiyama, D. (2007). Observation of Diffusion Behavior of Trace Elements in Hardened Cement Pastes by LA-ICP-MS, *Scientific Basis for Nuclear Waste Management XXXI (Material Research Society Symposium Proceedings volume 1107)*, pp. 585-592, ISBN 978-1-60511-079-0, Sheffield, UK, September 2007.

Chida, T. & Sugiyama, D. (2008). Diffusion Behavior of Organic Carbon and Iodine in Low-heat Portland Cement Containing Fly Ash, *Scientific Basis for Nuclear Waste Management XXXII (Material Research Society Symposium Proceedings volume 1124)*, pp. 379-384, ISBN 978-1-60511-096-7, Boston, USA, December 2008.

Glasser, F.P.; Macphee, D.E. & Lachowski, E.E. (1987). Modelling Approach to the Prediction of Equilibrium Phase Distribution in Slag-cement Blends and Their Solubility Properties, *Scientific Basis for Nuclear Waste Management XI (Material Research Society Symposium Proceedings volume 112)*, pp. 3-12, ISBN 0-931837-82-0, Boston, USA, December 1987.

Glasser, F.P.; Adenot, F.; Bloem Bredy, P.J.C.; Fachinger, J.; Sneyers, A.; Marx, G.; Brodersen, K.; Cowper, M.; Tyrer, M. et al. (2001). *Barrier Performance of Cements and Concretes in Nuclear Waste Management*, Final Report for CEC Contract FI4W-CT96-0030, EUR 19780 EN, 2001.

Haga, K.; Sutou, S.; Hironaga, M.; Tanaka, S. & Nagasaki, S. (2005). Effects of Porosity on Leaching of Ca from Hardened Ordinary Portland Cement Paste, *Cement and Concrete Research*, Volume 35, Issue 9, (September 2005), pp. 1764-1775, ISSN 0008-8846.

Harris, A.W.; Atkinson, A.; Balek, V.; Brodersen, K.; Cole, G.B.; Haworth, A.; Malek, Z.; Nickerson, A.K.; Nilsson, K. & Smith, A.C. (1998). *The Performance of Cementitious Barriers in Repositories*, Final Report for CEC Contract FI2W-0040, EUR 16643 EN, 1998.

Hindmarsh, A.C. & Gresho, P.M. (1984). The Stability of Explicit Euler Time-Integration for Certain Finite Difference Approximations of the Multi-Dimensional Advection-Diffusion Equation, *International Journal for Numerical Methods in Fluids*, Volume 4, Issue 9, (September 1984), pp. 853-897, ISSN 1097-0363.

Kurashige, I. & Hironaga, M. (2007). *Mechanism of Leaching Inhibition of Cementitious Materials due to Hydrogencarbonate Ion in Groundwater*, CRIEPI Report N06028, April 2007 [in Japanese with English Abstract], ISBN 4-86216-502-8.

Lagneau, V. & van der Lee, J. (2005). Simulation of Clogging Effects at the Interface between MX80-clay and Concrete in a Deep Radioactive Waste Repository, *Migration '05*, Avignon, France, September 2005.

Marty, N.C.M.; Tournassat, C.; Burnol, A.; Giffaut, E. & Gaucher, E.C. (2009). Influence of Reaction Kinetics and Mesh Refinement on the Numerical Modelling of Concrete/Clay Interactions, *Journal of Hydrology*, Volume 364, Issues 1-2, (15 January 2009), pp. 58-72, ISSN 0022-1694.

Parkhurst D.L. et al. (1980). *PHREEQE - A Computer Program for Geochemical Calculations*, U.S. Geological Survey.

Promentilla, M.A.B.; Sugiyama, T.; Hitomi, T. & Takeda, N. (2009). Quantification of Tortuosity in Hardened Cement Pastes Using Synchrotron-based X-ray Computed Microtomography, *Cement and Concrete Research*, Volume 39, Issue 6, (June 2009), pp. 548-557, ISSN 0008-8846.

Sousa, E. (2003). The Controversial Stability Analysis, *Applied Mathematics and Computation*, Volume 145, Issues 2-3, (25 December 2003), pp. 777–794, ISSN 0096-3003.

Sugiyama, D. (2008). Chemical Alteration of Calcium Silicate Hydrate (C–S–H) in Sodium Chloride Solution, *Cement and Concrete Research*, Volume 38, Issue 11, (November 2008), pp. 1270-1275, ISSN 0008-8846.

Sugiyama, D. & Fujita, T. (2006). A Thermodynamic Model of Dissolution and Precipitation of Calcium Silicate Hydrates, *Cement and Concrete Research*, Volume 36, Issue 2, (February 2006), pp. 227-237, ISSN 0008-8846.

Sugiyama, D.; Fujita, T.; Chida, T. & Tsukamto, M. (2007). Alteration of Fractured Cementitious Materials, *Cement and Concrete Research*, Volume 37, Issue 8, (August 2007), pp. 1257-1264, ISSN 0008-8846.

Sugiyama, D.; Chida, T. & Cowper, M. (2008). Laser Ablation Microprobe Inductively Coupled Plasma Mass Spectrometry Study on Diffusion of Uranium into Cement

Materials, *Radiochimica Acta*, Volume 96, Issue 9-11, Migration 2007, pp. 747-752, ISSN 0033-8230.

Taylor, H.F.W. (1997). *Cement Chemistry 2nd ed.*, Thomas Telford Services Ltd., p. 224, ISBN 0-7277-2592-0, London.

TRU Coordination Office (Japan Nuclear Cycle Development Institute and The Federation of Electric Power Companies) (2000). *Progress Report on Disposal Concept for TRU Waste in Japan*, JNC TY1400 2000-002, TRU TR-2000-02, March 2000.

Yasuda, K.; Yokozeki, K.; Kawata, Y. & Yoshizawa, Y. (2002). Physical and Transportation Properties of Concrete due to Calcium Leaching, *Cement Science and Concrete Technology*, Japan Cement Association, Volume 56, pp. 492-498, ISSN 0916-3182. [in Japanese with English Abstract].

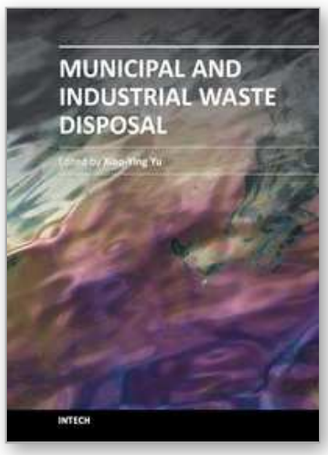

Municipal and Industrial Waste Disposal

Edited by Dr. Xiao-Ying Yu

ISBN 978-953-51-0501-5
Hard cover, 242 pages
Publisher InTech
Published online 11, April, 2012
Published in print edition April, 2012

This book reports research findings on several interesting topics in waste disposal including geophysical methods in site studies, municipal solid waste disposal site investigation, integrated study of contamination flow path at a waste disposal site, nuclear waste disposal, case studies of disposal of municipal wastes in different environments and locations, and emissions related to waste disposal.

How to reference

In order to correctly reference this scholarly work, feel free to copy and paste the following:

Daisuke Sugiyama (2012). Modelling of Chemical Alteration of Cement Materials in Radioactive Waste Repository Environment, Municipal and Industrial Waste Disposal, Dr. Xiao-Ying Yu (Ed.), ISBN: 978-953-51-0501-5, InTech, Available from: http://www.intechopen.com/books/municipal-and-industrial-waste-disposal/chemical-alteration-of-cement-materials-in-radioactive-waste-repository-environment

INTECH
open science | open minds

InTech Europe
University Campus STeP Ri
Slavka Krautzeka 83/A
51000 Rijeka, Croatia
Phone: +385 (51) 770 447
Fax: +385 (51) 686 166
www.intechopen.com

InTech China
Unit 405, Office Block, Hotel Equatorial Shanghai
No.65, Yan An Road (West), Shanghai, 200040, China
中国上海市延安西路65号上海国际贵都大饭店办公楼405单元
Phone: +86-21-62489820
Fax: +86-21-62489821

IntechOpen